Strong influence of lunar crustal fields on the solar wind flow

Charles Lue,[1,2] Yoshifumi Futaana,[1] Stas Barabash,[1] Martin Wieser,[1] Mats Holmström,[1] Anil Bhardwaj,[3] M. B. Dhanya,[3] and Peter Wurz[4]

Received 18 November 2010; revised 15 December 2010; accepted 28 December 2010; published 3 February 2011.

[1] We discuss the influence of lunar magnetic anomalies on the solar wind and on the lunar surface, based on maps of solar wind proton fluxes deflected by the magnetic anomalies. The maps are produced using data from the Solar WInd Monitor (SWIM) onboard the Chandrayaan-1 spacecraft. We find a high deflection efficiency (average ~10%, locally ~50%) over the large-scale (>1000 km) regions of magnetic anomalies. Deflections are also detected over weak (<3 nT at 30 km altitude) and small-scale (<100 km) magnetic anomalies, which might be explained by charge separation and the resulting electric potential. Strong deflection from a wide area implies that the magnetic anomalies act as a magnetosphere-like obstacle, affecting the upstream solar wind. It also reduces the implantation rate of the solar wind protons to the lunar surface, which may affect space weathering near the magnetic anomalies.
Citation: Lue, C., Y. Futaana, S. Barabash, M. Wieser, M. Holmström, A. Bhardwaj, M. B. Dhanya, and P. Wurz (2011), Strong influence of lunar crustal fields on the solar wind flow, *Geophys. Res. Lett.*, *38*, L03202, doi:10.1029/2010GL046215.

1. Introduction

[2] The Moon has neither a strong, global magnetic field nor a dense atmosphere, and the solar wind is mainly absorbed by the lunar regolith. However, there are regions of magnetized crust, called magnetic anomalies. Various measurements have indicated that the magnetic anomalies may interact with the solar wind [e.g., *Russell and Lichtenstein*, 1975]. The formation of bow-shocks [*Lin et al.*, 1998] and plasma-voids [*Halekas et al.*, 2008] above magnetic anomalies were suggested from in-situ magnetic field and electron measurements. Such features were also reproduced in multi-fluid MHD simulations [e.g., *Harnett and Winglee*, 2000]. However, our understanding of the interaction and the formation of mini-magnetospheres is very limited, especially from a global perspective. This is mainly because previous works are based on in-situ observations that are limited in space and time.

[3] Recently, *Futaana et al.* [2006] suggested a method of imaging mini-magnetospheres using neutral atom flux from the regolith. The idea is that a reduction in neutral atoms produced by the interaction between the solar wind and the lunar surface is expected above mini-magnetospheres. Using this idea and neutral atoms data from the Chandrayaan-1 lunar orbiter, *Wieser et al.* [2010] directly imaged a mini-magnetosphere, indicating a ~50% reduction of impinging solar wind ions over the strong magnetic anomaly at the Crisium antipode.

[4] Not only neutral atom observations, but also plasma observations can provide morphological information of the interaction. *Futaana et al.* [2003] suggested proton reflection from magnetic anomalies, to explain non-solar wind protons found by Nozomi, at ~2800 km from the lunar surface. *Saito et al.* [2010] identified a >10% reflection of the solar wind protons from some magnetic anomalies, using observations by Kaguya at an altitude <100 km. In this study, we use ion data from Chandrayaan-1 to map such protons associated with magnetic anomalies, to investigate the influence of the lunar magnetic anomalies on the solar wind and on the lunar surface.

2. Instrumentation and Data

[5] We used data from the Solar WInd Monitor (SWIM) [*McCann et al.*, 2007], which was carried by Chandrayaan-1 as part of the Sub-keV Atom Reflecting Analyzer (SARA) instrument [*Barabash et al.*, 2009]. The data was collected during 15 days between 19 April 2009 and 4 May 2009.

[6] During the observation period, the Moon was outside the Earth's bow shock, i.e., exposed to the undisturbed solar wind (Figure 1a). Chandrayaan-1 had a 100 km polar orbit. The solar zenith angle at equator crossings varied between 55° and 45°. The rotation of the Moon during the half month period provided >180° longitudinal coverage, mainly of the lunar far side (Figure 1b).

[7] SWIM measured positively charged particles in the energy range of 100 eV to 3 keV, with an energy resolution of $\Delta E/E$ ~7%, a mass resolution of $\Delta m/m$ ~50% and a time resolution of 8 s. The Field of View (FoV) was 9° × 180°, divided into 16 direction channels. The angular resolution was 7.5° × 10° (FWHM). For the nominal spacecraft attitude, the SWIM FoV spanned from nadir to zenith, perpendicular to the spacecraft velocity vector (see Figure 1b).

[8] SWIM data were collected on the dayside and filtered to not include cases when the spacecraft attitude deviated by more than 10° from the nominal nadir pointing. WIND data available from the MIT Space Plasma Group (http://web.mit.edu/space/www/) were used to evaluate the solar wind conditions. We removed all extreme cases, considering the SWIM measurements only when the solar wind flux was within the range from 0.8×10^8 cm^{-2} s^{-1} to 3.5×10^8 cm^{-2} s^{-1}. The averaged value was 1.8×10^8 cm^{-2} s^{-1} with the standard deviation 5.2×10^7 cm^{-2} s^{-1}.

3. Observations

[9] Figure 2 shows an example of SWIM observations obtained over the Imbrium antipode magnetic anomaly.

[1]Swedish Institute of Space Physics, Kiruna, Sweden.
[2]Department of Space Science, Luleå University of Technology, Kiruna, Sweden.
[3]Space Physics Laboratory, Vikram Sarabhai Space Center, Trivandrum, India.
[4]Physikalisches Institut, University of Bern, Bern, Switzerland.

0094-8276/11/2010GL046215

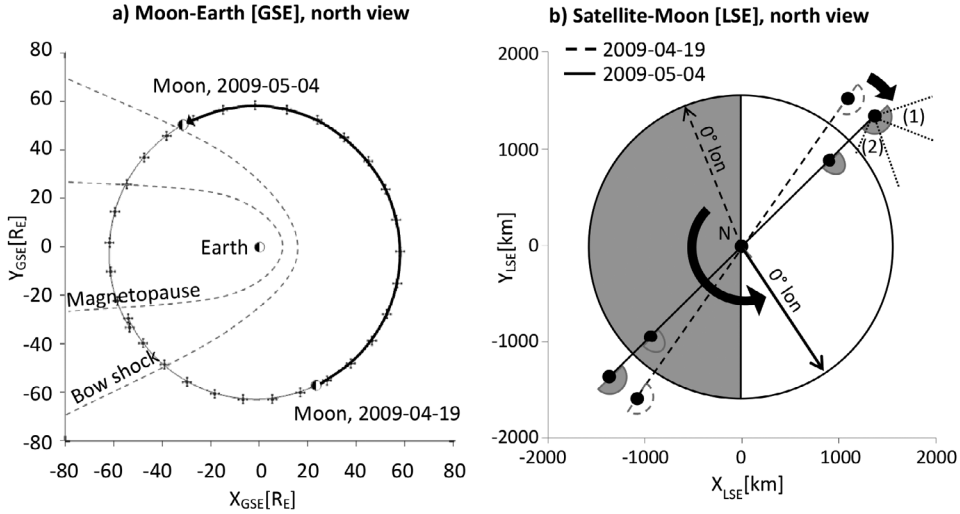

Figure 1. (a) The position of the Moon in the geocentric solar ecliptic (GSE) coordinate system for the studied period between 19 April and 4 May, 2009. The modeled bow shock [*Fairfield*, 1971] and magnetopause [*Shue et al.*, 1997] positions are shown with dashed lines. (b) The orbit of the Chandrayaan-1 spacecraft, in lunar-centered solar ecliptic (LSE) coordinates, projected to the ecliptic plane for the same time period as in Figure 1a. Selenographic 0-longitude (Earth-pointing) and spacecraft orbits are indicated with dashed lines for the beginning of the period and solid lines for the end of the period. Thick arrows illustrate the rotation of the Moon and the orbit in the LSE frame. The filled fan shapes illustrate the field of view of the SWIM sensor. The dotted lines show the separation of space pointing directions (1) and surface/horizon pointing directions (2).

From space-pointing directions (Figure 2a), the instrument observes the solar wind as the spacecraft passes the equator. Due to the viewing geometry of SWIM (Figure 1b), the SWIM sensor points away from the solar wind velocity vector at higher latitudes, so the solar wind cannot be seen, as discussed by *Futaana et al.* [2010]. We can see significant flux from surface- and horizon-pointing directions (Figure 2b). Because only cases with moderate solar wind flux and nominal attitudes were chosen, the observed large variations of more than three orders of magnitude in ions from these directions cannot be attributed to solar wind or attitude variations. Instead, a correlation is seen between Figures 2b and 2d, indicating that the variations result from the effect of the anomaly. In Figure 2b, there is no significant flux from unmagnetized regions, where surface-backscattered protons are reported by *Saito et al.* [2008]. This is likely because we used near horizon-looking directions, while surface-backscattered protons are expected from near nadir-looking directions. Therefore, we concluded that these protons are deflected by the magnetic anomalies. These deflected protons have the same energy as the solar wind protons, but are clearly heated. The Maxwellian fit gives a temperature of 270'000 K, while the solar wind temperature is about 19'000 K. The directional spread (FWHM) of the deflected protons is 30° compared to the solar wind (FWHM = 20°), as indicated in Figure 2c. The measured angular width of the solar wind is larger than the anticipated value from the temperature measurements (7°) due to the finite angular resolution of the sensor. For the same reason, the measured angular width of the deflected proton flux is also larger than the expected value from the temperature measurements (22°).

[10] Using the 15 day data period, we created a map of the observed deflected proton flux (Figure 3). For each 8 s observation, we used the peak value of the deflected differential flux observed by the instrument. The flux was mapped to the surface intersection point of the line-of-sight for the central direction of the sensor channel where highest flux was observed below horizon. This is 63° from the nadir. The use of the line-of-sight is reasonable because the proton gyro radius is large (~1300 km for a proton velocity of ~380 km/s and in IMF strength of ~3 nT) compared to the altitude (100 km) of the spacecraft. On the map, a clear correlation to the magnetic anomalies can be identified. Not only the clustered, strong anomalies but also isolated, weak anomalies (<3 nT at 30 km) appear on the proton map.

4. Deflection Efficiency

[11] Figure 4 shows the deflection ratio, i.e., the ratio between the incident solar wind flux and the flux which is deflected away from the lunar surface. The incident solar wind was retrieved from WIND data (with a delay of 1 hour, accounting for the travelling time between WIND and the Moon) and was adjusted by the cosine of the solar zenith angle. The deflected flux was calculated by multiplying the differential flux (Figure 3) with a solid angle of 0.15 sr, equivalent to the 22° angular spread estimated from the observed temperature (see section 3).

[12] Integrating the deflected flux over the far-side surface gives 2.2×10^{23} protons/s leaving the Moon. For the time period in question, the averaged solar wind flux measured by WIND was 1.8×10^{8} cm^{-2}s^{-1}. Multiplied by the Moon's cross-section, this gives a total of 1.7×10^{25} protons/s impacting on the Moon, resulting in ~1% deflection over the

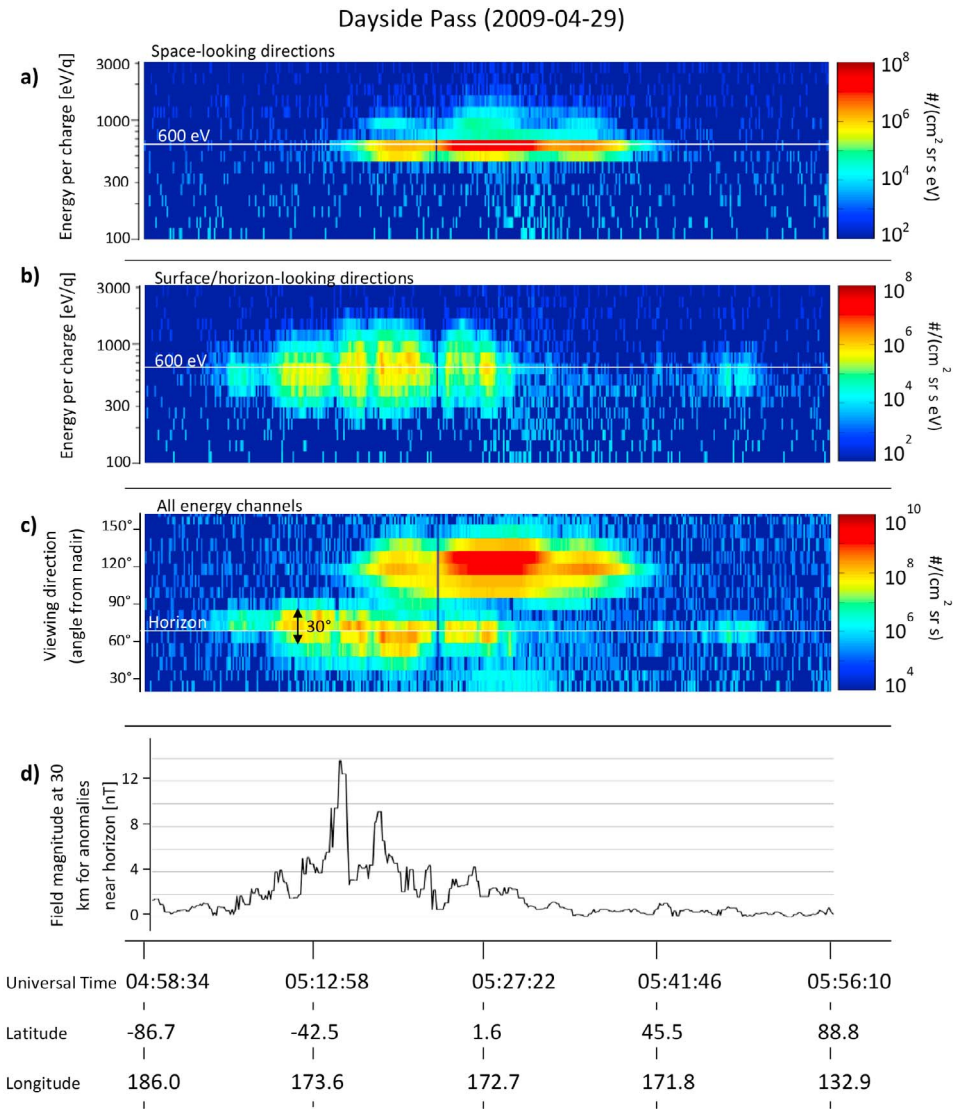

Figure 2. Dayside pass between 04:58 and 05:57 on 29 April 2009, over the Imbrium antipode magnetic anomalies. The energy distribution of the differential flux, summed over (a) five space-pointing directions (104°–142° from nadir) and (b) five surface-pointing directions (44°–80° from nadir). (c) The direction distributions in angle from nadir, of the differential flux, integrated over the 100 eV – 3 keV energy range. (d) For reference, the strength of magnetic anomalies near the horizon. The strength is given in field magnitude at 30 km altitude, in model by *Purucker* [2008], from Lunar Prospector data. Time and selenographical coordinates are also shown.

far-side. Limiting the integration to the regions where the deflected fluxes are observed (10% of the far-side area), we get an average deflection efficiency of ~10%. In the regions of strongest deflection (0.1% of the far-side area), the average deflection fraction is calculated to be ~50% (see also Figure 4).

5. Discussion and Conclusions

[13] On the scale of an individual anomaly, we deal with the transition plasma regime between MHD and the kinetic approximation when electrons are magnetized (gyro radius of 0.6–6 km for a temperature of 30 eV in a field of 3–30 nT) but protons not (gyro radius of 110–1100 km for 600 eV energy in a field of 3–30 nT). Therefore, magnetic reflection for protons should not occur. Since observations at lower altitudes with a full field of view and a complete plasma package would be required to investigate the physical mechanism in detail, we can only outline the basic scenario as follows. Magnetized electrons are deflected by the magnetic field gradient and set up a charge separation (because protons are non-magnetized), resulting in an ambipolar electric field. The related potential repels a fraction of the protons. Therefore, the deflection can take place not only over the strongest magnetic anomalies where the protons can be magnetized, but (although at a lower efficiency) also at weak, isolated anomalies of <3 nT at 30 km altitude, with a width of <100 km. Similar charge separation scenarios have been discussed in early studies based on Apollo 12 surface observations [e.g., *Neugebauer et al.*, 1972], and in a recent review paper by *Halekas et al.* [2010].

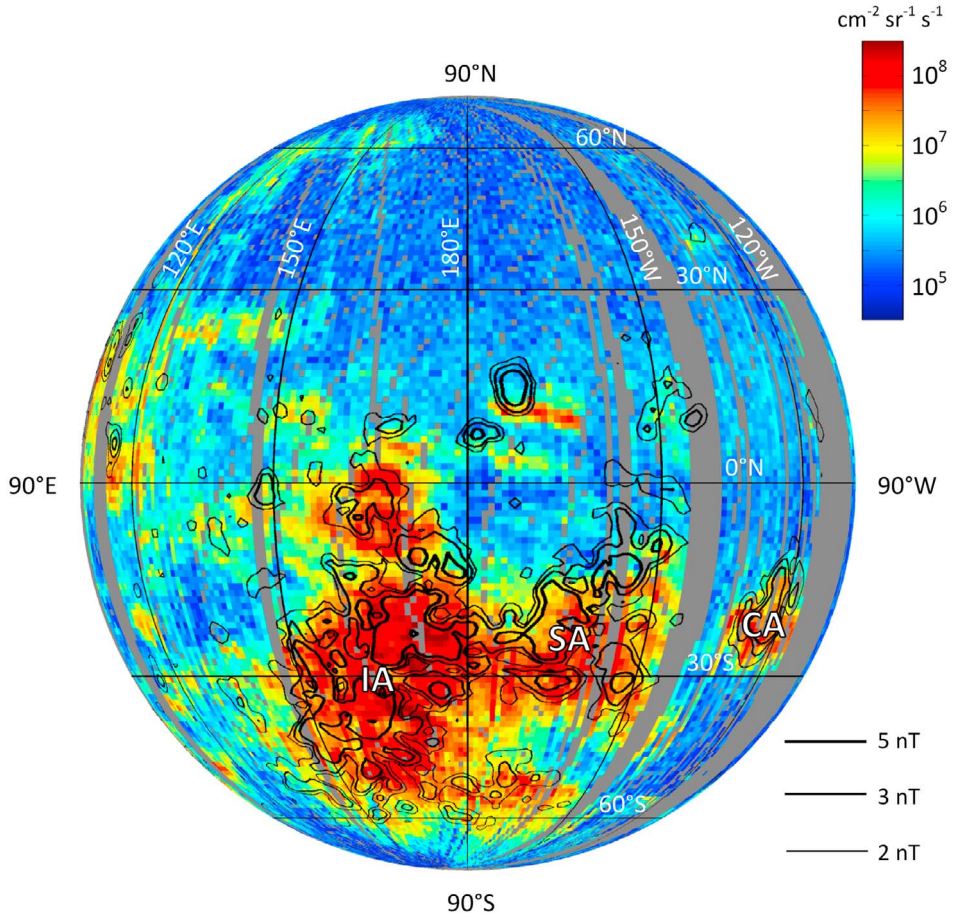

Figure 3. Map of observed deflected protons in the 200 eV – 1.7 keV energy range. The peak differential flux of protons is traced linearly to the surface of the Moon and binned to a 1° × 1° resolution. No interpolation or smoothing is applied. Black contours show 2 nT, 3 nT and 5 nT magnetic field strength at 30 km altitude in model by *Purucker* [2008].The large anomaly cluster at the Imbrium Antipode (IA) is clearly seen, as well as the Serenitatis Antipode (SA), Crisium Antipode (CA) and several smaller magnetic anomalies.

[14] The deflected protons create an anti-streaming flux of protons in the solar wind that results in a two-stream instability, wave-generation, and eventual heating of plasma. The protons can also be picked-up and accelerated by the solar wind [*Saito et al.*, 2008], which may take them into the lunar wake [*Nishino et al.*, 2009] or upstream of the Moon [*Holmström et al.*, 2010].

[15] Deflection efficiencies were estimated at ~1% for the entire far-side hemisphere, ~10% for the whole anomaly region (10% of the area), and ~50% for the strongest anomalies (0.1% of the area). These efficiencies correspond well to other studies, namely, >10% reflection for magnetic anomalies reported by *Saito et al.* [2010] for individual cases, and up to 50% reduction in impinging proton flux for a strong magnetic anomaly reported by *Wieser et al.* [2010] using ENA techniques.

[16] Regardless of the deflection mechanism for protons, the high solar wind deflection and reflection rates, as ions and neutral atoms, imply a lower proton implantation rate in the regolith at magnetic anomalies that may alter the space weathering compared to the surrounding areas. Moreover, it might affect the production of OH/H_2O in the outermost layer of the regolith via transfer of solar wind-implanted protons to the mineral-bound oxygen [*Pieters et al.*, 2009].

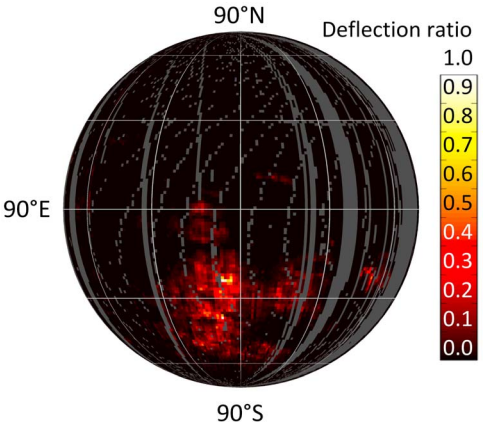

Figure 4. Map of the ratio between outflowing proton flux calculated from SWIM data and inflowing proton flux calculated from WIND data. The mapping procedure is the same as in Figure 3.

[17] *Halekas et al.* [2006], using earlier arguments by *Greenstadt* [1971], argued that large groups of anomalies may act in a coherent manner, forming a magnetosphere-like obstacle. Our study indicates that this is the case. Such groups deflect the solar wind flow on a scale of more than 1000 km that by far exceeds the typical proton gyro radius in a single-anomaly field. The energy density corresponding to a deflection efficiency of 10% is 10 times the magnetic field energy carried by the solar wind and thus a large reservoir of free energy. The questions to be addressed in future studies both theoretical and experimental is how this energy is transferred to the solar wind flow and whether or not it can result in the formation of a bow shock.

[18] **Acknowledgments.** Solar wind parameters from the WIND spacecraft were used as a reference for this study. The authors thank K.W. Ogilvie (NASA/GSFC) and A.J. Lazarus (MIT) for providing WIND data. This work has been supported by the Swedish Research Links Programme funded by the Swedish International Development Cooperation Agency (SIDA).

References

Barabash, S., et al. (2009), Investigation of the solar wind-Moon interaction onboard Chandrayaan-1 mission with the SARA experiment, *Curr. Sci.*, *96*(4), 526–532.

Fairfield, D. H. (1971), Average and unusual locations of the Earth's magnetopause and bow shock, *J. Geophys. Res.*, *76*, 6700–6716, doi:10.1029/JA076i028p06700.

Futaana, Y., S. Machida, Y. Saito, A. Matsuoka, and H. Hayakawa (2003), Moon-related nonthermal ions observed by Nozomi: Species, sources, and generation mechanisms, *J. Geophys. Res.*, *108*(A1), 1025, doi:10.1029/2002JA009366.

Futaana, Y., S. Barabash, M. Holmström, and A. Bhardwaj (2006), Low energy neutral atoms imaging of the Moon, *Planet. Space Sci.*, *54*(2), 132–143, doi:10.1016/j.pss.2005.10.010.

Futaana, Y., S. Barabash, M. Wieser, M. Holmström, A. Bhardwaj, M. B. Dhanya, R. Sridharan, P. Wurz, A. Schaufelberger, and K. Asamura (2010), Protons in the near-lunar wake observed by the Sub-keV atom reflection analyzer on board Chandrayaan-1, *J. Geophys. Res.*, *115*, A10248, doi:10.1029/2010JA015264.

Greenstadt, E. W. (1971), Conditions for magnetic interaction of asteroids with the solar wind, *Icarus*, *14*, 374–381, doi:10.1016/0019-1035(71)90008-X.

Halekas, J. S., D. A. Brain, D. L. Mitchell, R. P. Lin, and L. Harrison (2006), On the occurrence of magnetic enhancements caused by solar wind interaction with lunar crustal fields, *Geophys. Res. Lett.*, *33*, L08106, doi:10.1029/2006GL025931.

Halekas, J. S., G. T. Delory, D. A. Brain, R. P. Lin, and D. L. Mitchell (2008), Density cavity observed over a strong lunar crustal magnetic anomaly in the solar wind: A mini-magnetosphere?, *Planet. Space Sci.*, *56*(7), 941–946, doi:10.1016/j.pss.2008.01.008.

Halekas, J. S., Y. Saito, G. T. Delory, and W. M. Farrell (2010), New views of the lunar plasma environment, *Planet. Space Sci.*, doi:10.1016/j.pss.2010.08.011, in press.

Harnett, E., and R. Winglee (2000), Two dimensional MHD simulation of the solar wind interaction with magnetic field anomalies on the surface of the Moon, *J. Geophys. Res.*, *105*, 24,997–25,007, doi:10.1029/2000JA000074.

Holmström, M., M. Wieser, S. Barabash, Y. Futaana, and A. Bhardwaj (2010), Dynamics of solar wind protons reflected by the Moon, *J. Geophys. Res.*, *115*, A06206, doi:10.1029/2009JA014843.

Lin, R. P., D. L. Mitchell, D. W. Curtis, K. A. Anderson, C. W. Carlson, J. McFadden, M. H. Acuña, L. L. Hood, and A. Binder (1998), Lunar surface magnetic fields and their interaction with the solar wind: Results from Lunar Prospector, *Science*, *281*, 1480–1484, doi:10.1126/science.281.5382.1480.

McCann, D., S. Barabash, H. Nilsson, and A. Bhardwaj (2007), Miniature ion mass analyser, *Planet. Space Sci.*, *55*, 1190–1196, doi:10.1016/j.pss.2006.11.020.

Neugebauer, M., C. W. Snyder, D. R. Clay, and B. E. Goldstein (1972), Solar wind observations on the lunar surface with the Apollo-12 ALSEP, *Planet. Space Sci.*, *20*, 1577–1591, doi:10.1016/0032-0633(72)90184-5.

Nishino, M. N., et al. (2009), Solar-wind proton access deep into the near-Moon wake, *Geophys. Res. Lett.*, *36*, L16103, doi:10.1029/2009GL039444.

Pieters, C. M., et al. (2009), Character and spatial distribution of OH/H2O on the surface of the Moon seen by M3 on Chandrayaan-1, *Science*, *326*, 568–572, doi:10.1126/science.1178658.

Purucker, M. E. (2008), A global model of the internal magnetic field of the Moon based on Lunar Prospector magnetometer observations, *Icarus*, *197*, 19–23, doi:10.1016/j.icarus.2008.03.016.

Russell, C. T., and B. R. Lichtenstein (1975), On the source of lunar limb compressions, *J. Geophys. Res.*, *80*, 4700–4711, doi:10.1029/JA080i034p04700.

Saito, Y., et al. (2008), Solar wind proton reflection at the lunar surface: Low energy ion measurement by MAP-PACE onboard SELENE (KAGUYA), *Geophys. Res. Lett.*, *35*, L24205, doi:10.1029/2008GL036077.

Saito, Y., et al. (2010), In-flight Performance and Initial Results of Plasma Energy Angle and Composition Experiment (PACE) on SELENE (Kaguya), *Space Sci. Rev.*, doi:10.1007/s11214-010-9647-x, in press.

Shue, J.-H., J. K. Chao, H. C. Fu, C. T. Russell, P. Song, K. K. Khurana, and H. J. Singer (1997), A new functional form to study the solar wind control of the magnetopause size and shape, *J. Geophys. Res.*, *102*, 9497–9511, doi:10.1029/97JA00196.

Wieser, M., S. Barabash, Y. Futaana, M. Holmström, A. Bhardwaj, R. Sridharan, M. B. Dhanya, A. Schaufelberger, P. Wurz, and K. Asamura (2010), First observation of a mini-magnetosphere above a lunar magnetic anomaly using energetic neutral atoms, *Geophys. Res. Lett.*, *37*, L05103, doi:10.1029/2009GL041721.

S. Barabash, Y. Futaana, M. Holmström, C. Lue, and M. Wieser, Swedish Institute of Space Physics, Box 812, SE-98128 Kiruna, Sweden. (charles.lue@irf.se)

A. Bhardwaj and M. B. Dhanya, Space Physics Laboratory, Vikram Sarabhai Space Center, Trivandrum 695 022, India.

P. Wurz, Physikalisches Institut, University of Bern, Sidlerstrasse 5, CH-3012 Bern, Switzerland.